Dalton Transactions

ROYAL SOCIETY OF CHEMISTRY

PAPER

View Article Online
View Journal | View Issue

Check for updates

Cite this: *Dalton Trans.*, 2025, **54**, 16718

Sodium phosphaethynolate as P-source for the synthesis of molecular rhodium phosphides: an exploratory study

Zhongshu Li, *†[a] Jaap E. Borger,†[b] Thomas L. Gianetti, [c] Fabian Müller,[b] Bruno Pribanic,[b] Peter Coburger *[d] and Hansjörg Grützmacher *[a,b]

Received 23rd September 2025,
Accepted 23rd September 2025

DOI: 10.1039/d5dt02274f

rsc.li/dalton

Molecular transition metal phosphides (TMPs) containing a Rh_2P_2 and unprecedented Rh_4P_4 core could be generated from Na[OCP] and rhodium(I) precursor complexes carrying the bischelating tropPPh_2 ligand. These reaction proceed through a formal P-transfer step (trop = 5*H*-dibenzo[*a*,*d*]cyclohepten-5-yl), which involves migration of the CO unit to the Rh(I) center. With the related tetradentate ligand trop$_3$P and tridentate ligand trop$_2$PPh the first neutral and anionic $[Rh_x(L)_n(PCO)_y]_z$ complexes containing up to two rhodium centers and three intact phosphaethynolate units. These complexes are inert against CO migration. The results demonstrate a large influence of the metal coordination sphere on product formation, and indicate that low-coordinate rhodium(I) precursors are most effective for the preparation of RhP complexes using Na[OCP] as P-source.

Introduction

Transition metal phosphide (TMP) nanomaterials have been identified as high-performing catalysts for electrocatalytic water splitting[1] and deoxygenation of bio-oil,[2] which may be of interest for the development of sustainable energy sources. Their variety in the structural composition and associated electronic structures is attractive as it provides for a handle on catalytic activity and material properties. Generally, TMPs can be divided into metal-rich phases containing M–M bonds and phosphide-rich phases with P–P bonds, which explains the broad range of structure types and consequently electronic properties. The synthesis of TMP bulk and nanomaterials mostly relies on the reaction of hazardous phosphorus sources such as PH_3, $P(SiMe_3)_3$, or P_4 with a suitable transition metal precursor under various reaction conditions, which frequently involve high temperatures.[3] Molecular TMP complexes (featuring preformed M–P bonds) can be used as single-source molecular precursors for the synthesis of nanoparticles.[2a,4] Their selective preparation, however, is challenging especially for phosphides of the late transition metals.[5]

Binary rhodium phosphides of composition Rh_2P, Rh_3P_2, Rh_4P_3, RhP_2, and RhP_3 have been reported (for a review see ref. 3*c*) and the structures of some of them are known since over 60 years.[6] Only recently, the remarkable properties of especially Rh_2P as component of catalytically active materials in electro-[7] and photocatalytic[8] water splitting, methanol oxidation,[9] hydrogenation and hydrodesulfurization,[10] hydroformulation,[11] and amination[12] has been discovered.

The development of large-scale syntheses of phosphaethynolate salts (M + $[OCP]^-$; M = K, Na)[13] has spurred the use of these salts as phosphorus containing small building blocks over the last decade.[14] In analogy to the isovalence electronic azide anion, the $[OCP]^-$ anion may serve as "P^-" transfer reagent under extrusion of CO (as suggested by the resonance structure $[O{\equiv}C \rightarrow P^-]$).[14,15] Salt metathesis reactions of Na[OCP] with metal halides show the phosphaethynolate anion to coordinate to d- and f-block metal centers either through the P- or O-binding site, producing stable monomeric compounds of the type A (M≡Re,[16] Co,[17] Cu,[17] Ag[18] and Au[17]) and B (M≡U,[19] Th,[19b] Sc,[20] Y,[21] Nd[21] and Sm[21]) or dinuclear complexes such as C (M = Fe)[22] or D (M = Nd,[21] Scheme 1a). These type of complexes may indeed afford metal phosphides through CO migration or release.[23] For example, the ligand-stabilized Ti_2P_2 **I**,[24] Ir_2P_2 **II**,[17] (for a related Pt_2P_2 complex see ref. 25), U_2P_2 **III**,[26] Ni_2P_2 **IV**,[27] Fe_2P_3 **V**[4b] and anionic $[WP]^-$ **VI**[28] could be prepared (Scheme 1b). Note that **V** proved to be a suitable molecular precursor for the preparation FeP nano-

[a]*LIFM, IGCME, School of Chemistry, Sun Yat-Sen University, Guangzhou 510006, China. E-mail: lizhsh6@mail.sysu.edu.cn*
[b]*Department of Chemistry and Applied Biosciences, ETH Zürich, Vladimir-Prelog-Weg 1, Hönggerberg, 8093 Zürich, Switzerland. E-mail: hgruetzmacher@ethz.ch*
[c]*Department of Chemistry and Biochemistry, University of Arizona, Tucson, Arizona 85721, USA*
[d]*Department of Inorganic Chemistry, TU München, Lichtenbergstraße 4, 85747 Garching, Germany. E-mail: peter.coburger@tum.de*
†These authors contributed equally to this work.

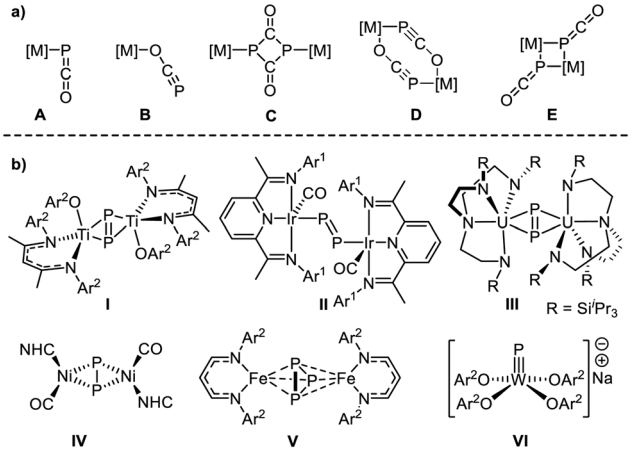

Scheme 1 (a) Structural motifs obtained from $[OCP]^-$ coordination to d- and f-block element centers. (b) Metal phosphide complexes obtained from Na[OCP] through CO migration or release. NHC = IPr or IMes, Ar1 = *m*-xylyl, Ar2 = Dipp.

particles that were found to be especially active as electrocatalysts on the anodic and cathodic side for water-splitting.[4b]

To the best of our knowledge, well-defined binary RhP phases or molecular rhodium phosphido complexes with a Rh : P ratio of 1 : 1 are unknown. Here we report the results of our attempts to prepare molecular Rh phosphide complexes using a variety of rhodium(I) precursor complexes and Na[OCP] as "P^-" transfer reagent. These reactions afforded the first Rh(PCO) adducts of the type **A** and **C**. Furthermore, a new type of a dinuclear complex with a central μ_2-$P_2(C{=}O)_2$ heterocycle was discovered. Finally the formation of polynuclear Rh_2P_2 and unprecedented Rh_4P_4 complexes with Rh and P in a 1 : 1 ratio is disclosed, whose electronic structures were analysed by DFT methods.

Results and discussion

In order to evaluate the influence of different coordination environments around a rhodium(I) centre in reactions with Na[OCP], various Rh–X precursor complexes were tested. Commercially available $[RhCl(PPh_3)_3]$ or $[Rh_2(\mu_2\text{-}Cl)_2(cod)_2]$ only gave black precipitates (likely Rh particles) and a variety of phosphorus compounds (detected by ^{31}P NMR), which were not identified. However, Rh(I) complexes with trop-substituted (trop = 5*H*-dibenzo[*a*,*d*]cyclohepten-5-yl) tetra-, tri- and bidentate phosphine ligands, which were prepared according to known procedures (see the SI for details),[29] reacted with Na[OCP] to give defined compounds.

First the saturated 18-valence electron configured [RhCl(Ptrop$_3$)] complex with a tetradentate tris(olefin) phosphine ligand, was reacted with Na[OCP] in dichloromethane (DCM) at room temperature. The instant formation of [Rh(PCO)(Ptrop$_3$)] **1** resulted from a salt metathesis reaction (Scheme 2), and a yield of 90% was obtained after work-up. The intact P-bound PCO entity shows a ^{31}P NMR resonance signal at δ = −346.9 ppm, (*cf.* $\delta^{31}P$ Na[OCP] = −391 ppm), which is in the middle of the rather broad range of ^{31}P NMR shifts observed for κ^1*P*-PCO bound complexes ($\delta^{31}P$ = −225.8 [Co(PDI)(PCO)] to −441.0 ppm ($[W(CO)_5(PCO)]^-$)).[14a] The resonance of the ^{31}P nucleus of the P═C═O ligand is split into a doublet of doublets by coupling with the ^{31}P nucleus of the trop$_3$P ligand in *trans*-position ($^2J_{P,P}$ = 138.5 Hz) and the directly bound ^{103}Rh nucleus ($^1J_{P,Rh}$ = 36.7 Hz). The ^{31}P nucleus of the trop$_3$P ligand shows likewise a doublet of doublet resonance but the $^1J_{P,Rh}$ coupling (138.5 Hz) is significantly larger. The asymmetric stretching frequency of the PCO ligand appears at ν_{asym}(PCO) = 1839 cm^{-1} in the IR spectrum, which is in the range of κ^1*P*-PCO bound ligands in other complexes.[14a] The related 18 valence electron complex $[RhCl(PPh_3)(HNtrop_2)]$ also reacts cleanly in a salt metathesis reaction with Na[OCP] to give the corresponding complex $[Rh(PCO)(PPh_3)(HNtrop_2)]$ **2**. Note that in the precursor complex the chlorido ligand is located in axial position, while in **2** the PCO ligand is located in equatorial position of the trigonal bipyramidal structure ($\delta^{31}P$ Rh(*P*CO) = −365.1 pm; ν_{asym}(PCO) = 1853 cm^{-1}), which is indicated by the small $^2J_{P,P}$ coupling constant (10.0 Hz) typical of a *cis*-arrangement Ph_3P–Rh–PCO (Scheme 2). This phenomenon was also observed when Cl^- is replaced with other weakly binding ligands such as $(O_3SCF_3)^-$ (OTf^-).[29a] Indeed, the Rh–PCO bond (2.493 Å) is remarkably long in comparison to the Rh–PPh_3 bond (2.269 Å) (for details see S3 in the SI).

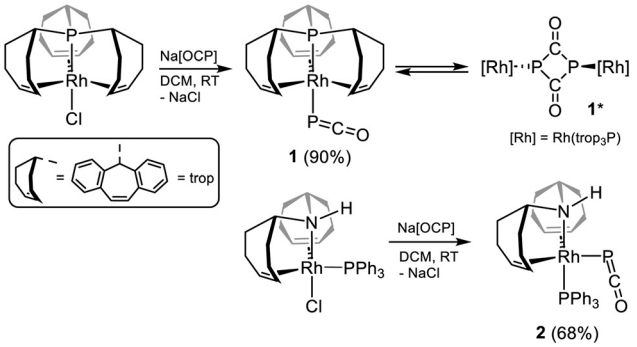

Scheme 2 Reaction of Na[OCP] with Rh(trop$_3$P)Cl to afford **1**, dimerization to **1*** and related complex **2**; trop = 5*H*-dibenzo[*a*,*d*]cyclohepten-5-yl.

Compound **1** is soluble in tetrahydrofuran (THF) and 1,2-dichlorobenzene, in which it is stable for at least 24 h at room temperature. With the aim of extruding CO, solutions of **1** in both solvents were heated to 70 °C and analyzed using ^{31}P NMR spectroscopy. Instead of decarbonylation, however, a dimerization towards $[Rh_2(Ptrop_3)_2[\mu_2\text{-}\kappa P,\kappa P'\text{-}(P_2C_2O_2)]]$ **1*** occurs. The formation of this complex with a bridging dianionic four-membered 1,3-diphosphacyclobutanyl-2,4-dione as-heterocycle, $[P_2(C{=}O)_2]^{2-}$, is indicated by the profound shift of the ^{31}P resonance to higher frequencies in the ^{31}P NMR spectrum ($^{31}P\delta$ = 183.0 ppm, $\Delta\delta$ = 530 ppm). A conversion of up to 30% can be reached after 18 h. UV irradiation of solutions of **1** gave the same result. It was not possible to achieve a higher

conversion rate even upon prolonged heating, which indicates an equilibrium between **1** and **1***, with a sizable barrier for interconversion. This is confirmed by DFT calculations (ωB97X-D/Def2-SVP),[30] which indicate that the process 2 **1** ⇆ **1*** is mildly exergonic by −7.0 kcal mol^{-1} with a barrier of $\Delta G^{\#}$ = 27.1 kcal mol^{-1} for the concerted [2 + 2]-dimerization.

In the next step, the dinuclear complex [Rh$_2$(μ$_2$-Cl)$_2$(trop$_2$PPh)$_2$]—featuring the tridentate trop$_2$PPh ligand instead of tetradentate trop$_3$P—was exposed to an excess of Na[OCP] in acetonitrile (MeCN) at room temperature (Scheme 3). Again no cleavage of the phosphorus-carbonyl bond could be observed. The reaction produced one major product within 24 h that directly precipitated as red powder from the reaction solution and was characterized as Na[**3**] (39% isolated yield) by multinuclear NMR spectroscopy, elemental analysis, and single crystal X-ray diffraction (XRD, Fig. 1b *vide infra*). Na[**3**] is sparingly soluble in THF and slowly decomposes in solution (see the SI). We propose that its formation proceeds *via* an Rh(PCO) adduct similar to **1**, which may then dimerize through coordination of the available P-lone pair at the PCO ligand to a rhodium center of a second unsaturated 16e [Rh(PCO)(PhPtrop$_2$)] fragment furnishing [**IMI**] with two μ$_2$-κ*P*-PCO moieties (Scheme 3; *cf.* **E**, Scheme 1). Subsequent nucleophilic attack of additional Na[OCP] at one of its carbonyl C-atoms then affords the final product. The ^{31}P chemical shift found for P1 at δ = −471.6 ppm is the most low frequency chemical shift reported for a PCO ligand to date. The other ^{31}P nuclei resonate at δ^{31}P = 53.0 ppm (P2), 266.6 ppm (P3), and 120.2 ppm (P4/P5).

Heating or UV/Vis irradiation of Na[**3**] in THF does not promote the elimination of CO. Like for **1** and **2**, we assume that the electronic saturation – all complexes discussed so far are 18 valence electron configured – may be the reason this inertness. We therefore chose the dinuclear complex [Rh$_2$(μ$_2$-Cl)$_2$(tropPPh$_2$)$_2$] as precursor complex, which contains 16 valence electron configured d^8-Rh(I) centers in a square planar coordination sphere. The stoichiometric reaction with Na[OCP] in acetonitrile at room temperature afforded [Rh$_2$(CO)$_2$(Ph$_2$Ptrop)$_2$(η^2-P$_2$)] **4**, which precipitated from the reaction solution allowing isolation in 35% yield after filtration and several washing steps (Scheme 3).

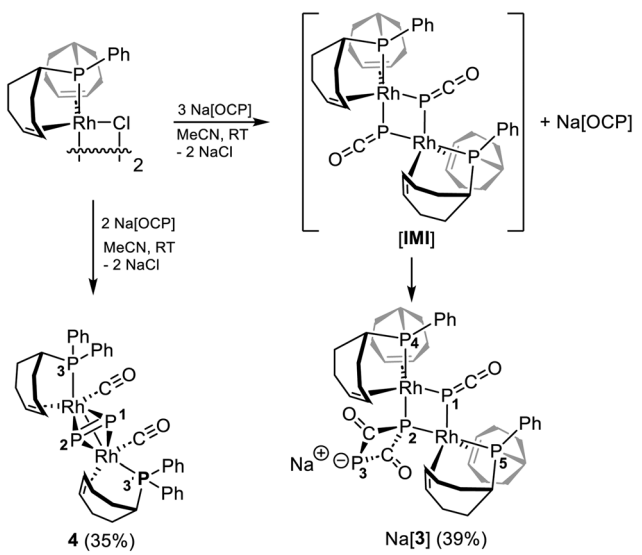

Scheme 3 Reaction of Na[OCP] with [Rh(trop$_2$PPh)Cl]$_2$ to afford Na[**3**] or **4**.

The absence of any ^{31}P NMR signals at low frequencies recorded for solutions of **4** show that no OCP unit remained intact. This is also indicated by the IR spectrum, which shows no absorptions in the region typical for coordinated OCP units (1841–1890 cm^{-1})[14a] but a strong absorption at ν_{sym}(CO) = 1966 cm^{-1} and a medium one at ν_{asym}(CO) = 1960 cm^{-1}, which are assigned to Rh ← CO carbonyl stretching vibrations. The ^{31}P nuclei P3 and P3′ of the Ph$_2$Ptrop ligand give rise to one signal at δ = 70.8 ppm (in [D$_8$]THF) indicating that these nuclei are magnetically equivalent and related by symmetry. Furthermore, two doublets are observed at ^{31}P δ = 102.1 ppm and 124.6 ppm and the large $^1J_{P,P}$ coupling constant of 540.7 Hz indicates a direct P–P bond. These spectroscopic data are consistent with the formula given for **4** in Scheme 4 and is confirmed by a XRD analysis (*vide infra*).

In solution, **4** is not stable and over the course of 24 h in THF at room temperature, partly converted to a new complex featuring a set of ^{1}H and ^{31}P NMR resonance signals corresponding to a Rh-coordinated tropPPh$_2$ ligand (δ^{31}P ≈ 70 ppm). In addition, one broad ^{31}P NMR signal emerged at δ = 119.8 ppm, which is in the same region as the signals originating from the P$_2$ bridge in **4** (see above). No further evolution of the signal ratios was observed after 24 h, not even upon heating the sample to 65 °C. A variable temperature ^{31}P NMR spectroscopy study in the range of T = −40–65 °C revealed a reversible process. At 65 °C a significant sharpening of the signals arising from both **4** and the newly formed product is observed, while at −40 °C multiple unidentified species are detected (see the SI for details). Although the exact nature of this process is as yet unclear, it is possible that these observations arise from an isomerization of *syn*-CO **4** to its C_2 symmetric *anti*-CO conformer which may involve a number of intermediates. A DFT calculations indicates that the energy difference between these two isomers is very small, $\Delta G_{syn\text{-CO }\mathbf{4} \rightarrow anti\text{-CO }\mathbf{4}}$ = 1.6 kcal·mol^{-1}.

Encouraged by the result obtained with the dinuclear complex [Rh$_2$(μ$_2$-Cl)$_2$(tropPPh$_2$)$_2$], we reacted the mononuclear Rh(I) complex [RhCl(Ph$_2$Ptrop)$_2$] with Na[OCP] in DME at room temperature. The result is shown in Scheme 4. The dark brown suspension was allowed to stir for 18 h and then filtered prior to removing the volatiles. The obtained black powder was washed with *n*-hexane and Et$_2$O and subsequently analyzed by ^{31}P NMR spectroscopy ([D$_6$]benzene). The recorded spectrum showed the formation of **4** as the major product, uncoordinated tropPPh$_2$ (δ = −14.1 ppm; see the SI), and a minor product that exhibits a broad doublet at δ = 64.2 ppm (J = 173.2 Hz) and a broad singlet at 41.0 ppm (1 : 1 ratio). Fortuitously, few black crystalline platelets of the latter could be isolated upon layering a solution of the crude product in

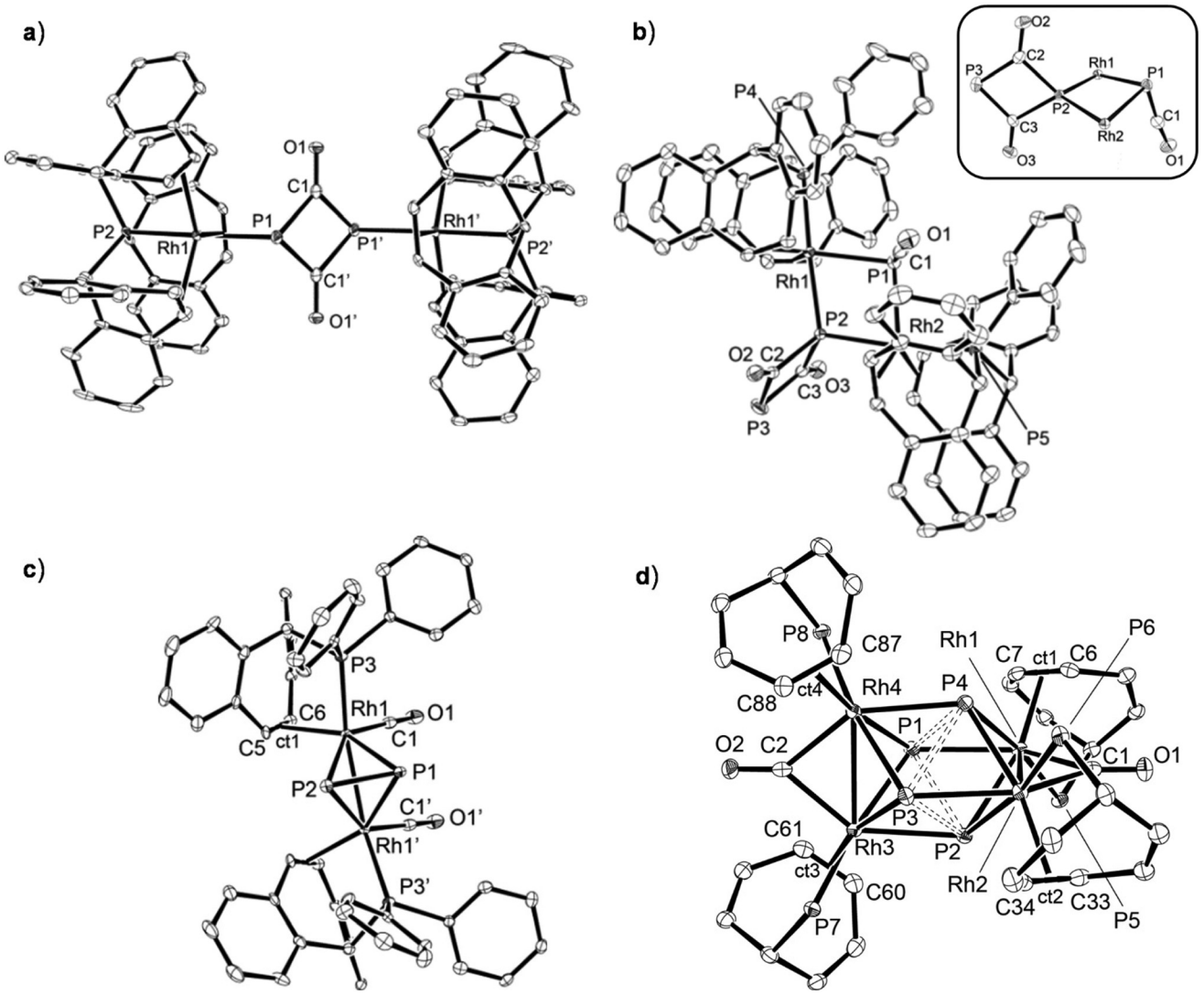

Fig. 1 Molecular structure (ellipsoids are shown at 50% probability) of (a) **1*** (hydrogen atoms and one 1,2-$Cl_2C_6H_4$ molecule are omitted for clarity). Selected bond distances [Å] and angles [°]: Rh1–P1 2.4257(16), Rh1–P2 2.1715(14), P1–C1 1.859(5), P1–C1′ 1.821(6), C1–O1 1.233(6), C1–P1–C1′ 80.3(3), P1–C1–P1′ 99.7(3), Rh1–P1–P1′ 120.85(9), P1–C1–P1′–C1′ –180.0(3). Symmetry operation: –*x*, –*y*, 2 – *z*. (b) [**3**]$^-$ (left) and its $Rh_2[P_2(C{=}O)_2](PCO)$ core, shown along the Rh–Rh axis (right) (hydrogen atoms, the $[Na(MeCN)_4]^+$ counter ion and two MeCN molecules are omitted for clarity). Selected bond distances [Å] and angles [°]: Rh1–P1 2.5072(7), Rh2–P1 2.4479(7), Rh1–P2 2.3622(6), Rh2–P2 2.3781(6), Rh1–P4 2.2781(6), P1–C1 1.657(3), P2–C2 1.888(3), P2–C3 1.889(3), P3–C2 1.799(3), P3–C3 1.798(3), Rh1–P2–Rh2 106.58(3), P2–Rh1–P1 74.71(2), P2–Rh2–P1 75.55(3), Rh1–P1–Rh2 100.14(3). (c) **4** (hydrogen atoms and a disordered THF molecule are omitted for clarity). Selected bond distances [Å] and angles [°]: Rh1–Rh1i 2.7606(11), P1–P2 2.066(2), Rh1–P3 2.2938(10), Rh1–C1 1.927(4), C1–O1 1.139(5), Rh1–P1 2.3803(11), Rh1–P2 2.4021(11), C5–C6 1.398(6), Rh1–ct1 2.194(3), Rh1–P2–P1–Rh1i 79.60(4). Symmetry operation: *x*, 3/2 – *y*, *z*. (d) **5** (hydrogen atoms, two benzyl and two phenyl rings per Ph_2Ptrop, and one Et_2O molecule are omitted for clarity). Selected bond distances [Å] and angles [°]: Rh1–Rh2 2.7673(3), Rh3–Rh4 2.7776(3), C1–O1 1.162(3), C2–O2 1.156(3), P1–Rh1 2.4671(6), P1–Rh3 2.4442(6), P1–Rh4 2.4243(6), P2–Rh1 2.3938(6), P2–Rh2 2.4312(6), P2–Rh3 2.4494(6), P3–Rh2 2.4547(6), P3–Rh3 2.3996(6), P3–Rh4 2.4337(6), P4–Rh1 2.4403(6), P4–Rh2 2.4036(6), P4–Rh4 2.4710(6), P1–P4 2.4759(9), P1–P2 2.5369(9), P3–P2 2.5529(9), P3–P4 2.5724(9), C6–C7 1.406(4), C33–C34 1.407(3), C60–C61 1.409(4), C87–C88 1.413(3), Rh1–ct1 2.1260(17), Rh2–ct2 2.1366(18), Rh3–ct3 2.1372(17), Rh4–ct4 2.1063(18).

DME with *n*-hexane and an XRD study allowed to determine also the structure of this minor product (*vide infra*) as a Rh_4P_4 cluster **5** shown in Scheme 4. Formally, **5** is the product of a dimerization reaction of **4** under loss of two equivalents of CO, 2 [**4**] → [**5**] + 2 CO. And although we failed to realize this process experimentally, DFT calculations show that it would be thermodynamically favored by $\Delta G = -16$ kcal mol^{-1}.

Structure determinations of compounds 1*–5

Single crystals of **1*** (orange), **2** (orange), **3** (red), **4** (orange), and **5** (dark brown) were grown and subjected to XRD analyses, which allowed to determine the structures of these compounds. The structural details of the PCO unit in **2** (P–C 1.532 Å, C–O 1.175 Å, P–C–O 176.9°) is in line with previous

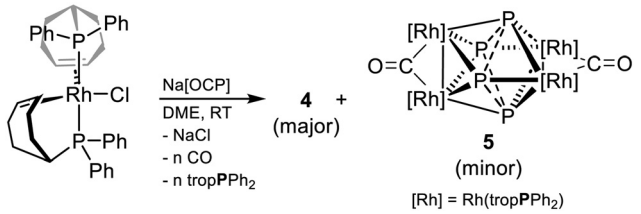

Scheme 4 Reaction of Na[OCP] with $Rh(tropPPh_2)_2Cl$ to afford the major product **4** and minor **5**.

reports on related M–PCO complexes[14a] and not discussed in detail here (for a structure plot see S3 in the SI). The molecular structure of **1*** (Fig. 1a) shows a central planar $P_2(C{=}O)_2$ heterocycle, which is located on a crystallographic inversion center [P1–C1–P1′–C1′ dihedral = −180.0(3)°]. The averaged P–C bond lengths within the P_2C_2 cycle (1.840 Å) and the C=O distances (1.233 Å) indicate P–C single and C=O double bond character.[31] As expected the C1–P1–C1′ angle (80.3°) is significantly smaller than the P1–C1–P1′ angle (99.7°) (overall the bond metrics are comparable to related main group-[13c,14,15,32] and transition metal-substituted[22] 1,3-diphosphacyclobutane-1,2-diones). The [Rh(Ptrop$_3$)] fragments deviate significantly out-of-plane from the planar $P_2(C{=}O)_2$ ring (Rh–P1–P1′ 120.85°) such that one fragment is located above and the other below the central ring. The sum of bond angles at P1, P1′ amount to 306.48° indicating a free electron pair at each P center. Consequently, the bond lengths between the Rh(I) center and the three-valent phosphorus center of the formally dianionic $[P_2(=O)_2]^{2-}$ ring are significantly longer (Rh–P1 2.426 Å) than the Rh–P2 bonds (2.172 Å), in which the pentavalent P2 center of the Ptrop$_3$ ligand is involved.

The mono-anionic part of the solid state structure of Na[**3**], and a plot of its unique $Rh_2[P_2(C{=}O)_2](PCO)$ core, are depicted in Fig. 1b (the $[Na(MeCN)_4]^+$ counter cation has a contact to O3 [Na1···O3 2.289(2) Å but is not shown for clarity)]. The anion $[\mathbf{3}]^-$ contains both a bridging μ_2-κ*P*-$[P_2(C{=}O)_2]^{2-}$ heterocycle and a bridging μ_2-κ*P*-P=C=O unit, which complete the distorted trigonal bipyramidal coordination spheres of each Rh(I) center. Under the assumption that both bridging ligands act as 4 electron donors, the Rh(I) centers achieve a valence electron count of 18. To our knowledge, for both coordination modes there is no precedence. The averaged Rh1/2–P1 bond lengths (2.477 Å) to the PCO ligand and the averaged Rh1/2–P2 bond lengths (2.372 Å) to the $P_2(C{=}O)_2$ heterocycle are again longer than the Rh1–P4 (2.278 Å) and Rh2–P5 (2.281 Å) bonds to the PhPtrop$_2$ ligand. Within the central Rh_2P_2 cycle, the bond angles at the bridging P centers [Rh1–P1–Rh2 100.14(3)°; Rh1–P2–Rh2 106.58(3)°] are much larger than at the Rh(I) centers [P1–Rh1–P2: 74.71(2)°; P1–Rh2–P2: 75.55(3)°]. In the 1,3-diphosphacyclobutane-2,4-dione moiety, the averaged P3–C2/C3 distances (1.79 Å) are much shorter than the ones involving the bridging P2 center (P2–C2/C3 = 1.89 Å) indicating significant π-electron delocalization over the C2–P3–C3 fragment. The μ_2-κ*P*-P=C=O unit has a P1–C1 bond length of 1.657(3) Å, which is significantly longer than the related one in **2** (1.522(4) Å; compare also P–C in $[Na(DME)_2]_2[\mu_2$-κ*O*-OCP$]_2$ = 1.589(3) Å)[13b] or other mononuclear κ*P*-PCO complexes (<1.64 Å).[14,15] This observation is in line with the assumption that the μ_2- κ*P*-bridging $[P{=}C{=}O]^-$ can act as 4 electron donor ligand (visualized by the resonance form $(P^{2-} \leftarrow C{\equiv}O^+)$).

The solid state structure of $[Rh_2(CO)_2(Ph_2Ptrop)_2(\eta^2\text{-}P_2)]$ **4** is shown in Fig. 1c. As indicated by the spectroscopic data, the CO units are not bound as PCO anymore, but have migrated to the Rh(I) centers as terminal carbonyl ligands binding in *cis*-positions with respect to the diphosphorus moiety. The P1–P2 bond is 2.066(2) Å long, a value that is similar to that observed in the related complex $[Rh_2(CO)_2(\mu\text{-dppm})_2(\mu,\eta^2\text{-}P_2)]$ (2.081(7) Å; dppm≡$CH_2(PPh_2)_2$),[33] and close to the predicted length of a P≡P double bond ($\sum r_{cov}$[P=P] = 2.04 Å).[31c] The P1–P2 axis is the mirror plane of the complex (in accord with the equivalence of the Ph_2Ptrop ligands in the NMR spectra) and almost perpendicular to the Rh1–Rh1′ axis [Rh1–P2–P1–Rh1′ torsion angle = 79.60(4)°]. The short Rh1–Rh1′ distance of 2.7606(11) Å indicates a bonding interaction between both metal centers and in combination with the Rh–P distances (2.39 Å; average) allow to describe **4** best as a Rh_2P_2 tetrahedron.

Finally, the XRD analysis of single crystals of **5** allowed the identification of a new Rh_4P_4 metal phosphido cluster. This is encapsulated by four bidentate Ph_2Ptrop ligands and by two bridging carbonyl groups (Fig. 1d). The Rh1–Rh2 and Rh3–Rh4 bonds are 2.772 Å (average) long and again correspond to single bonds. The Rh–P distances vary over a range from 2.394 to 2.471 Å and on the average (2.43 Å) are somewhat longer than in **4**. Most remarkable in the structure of **5** are the P1–P2 [2.5369(9)], P2–P3 [2.5529(9)], P3–P4 [2.5724(9) Å], and P4–P1 [2.4759(9) Å] distances, which are similar and unusually long (average: 2.53 Å). This value is significantly longer than sum of covalent radii ($\sum r_{cov}$[P–P] = 2.22 Å)[31c] but much smaller than the sum of van der Waals radii ($\sum r_{vdW}$[P, P] = 3.80 Å)[34] and in the same range as that reported for related $[(\eta^5\text{-Cp})_4Co_4P_4]$ (avg. P–P = 2.57 Å).[35] The Rh–Rh, Rh–P and P–P distances fall with the range determined for the phosphorus poor and rich binary phases RhP_2 and RhP_3.[36] Another interesting structural feature of **5** is that the distances between the Rh center and the coordinated olefinic units of the Ph_2Ptrop ligand are comparatively short (given by the average distances of the Rh centers to the centroids of the $C{=}C_{trop}$ units: Rh–ct = 2.13 Å). In contrast, the $C{=}C_{trop}$ distances relatively long (average 1.41 Å) when compared to **4** (Rh–Ct 2.194; C=Ctrop = 1.39 Å; *cf*. uncoordinated Ph_2Ptrop: 1.33 Å). These data reflect a high electron density within the Rh_4P_4 cluster leading on one side to long Rh–P and P–P bonds but on the other to significant electron donation from filled metal orbitals into the π* orbitals of the $C{=}C_{trop}$ units.

Analyses of the electronic structure of 4 and 5 by DFT calculations

Calculations used for the elucidation of the electronic structures of **4** (Rh_2P_2 cluster core) and **5** (Rh_4P_4 cluster core) were carried out with the ORCA program package[37] and details are

given in the SI. The calculated bond lengths correspond well with the experimentally determined ones (Tables S1 and S2 in the SI). The Mayer-bond order (MBOs) for the P═P bond (1.39) in the tetrahedral cluster **4** shows significant multiple bond character, while the Rh–P bonds (0.68, 0.70) correspond to single bonds. A significant bonding interaction between the rhodium centers is indicated by MBO_{Rh-Rh} = 0.38 (see Table S1 for a listing of the MBOs of **4**). Intrinsic bond orbitals (IBOs) have been successfully used to analyze the electronic structure of cluster compounds,[38] and for **4** six fully occupied orbitals which account for bonding within the Rh_2P_2 unit are obtained (Fig. 2).

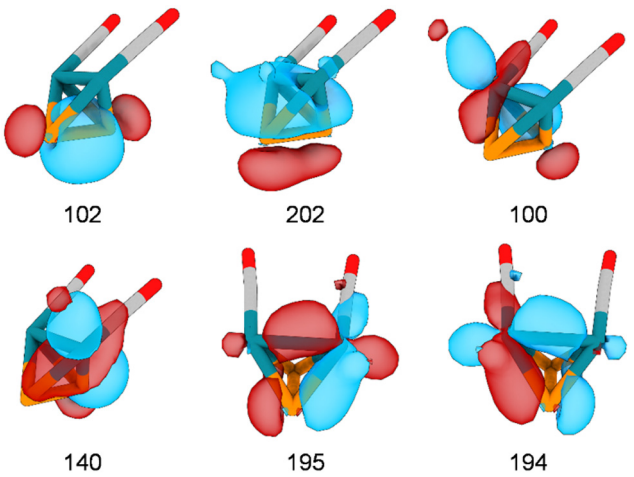

Fig. 2 Orbitals (occupied by two electrons) within the Rh_2P_2 unit accounting for bonding interactions between the cluster atoms (surface isovalue = 0.04, the orbital number is given for each orbital). Color code: C: grey, orange: P, petrol: Rh, red: oxygen.

Orbital number 102 represents the σ-bond between the P–P atoms, while orbital no. 202 corresponds mainly to a π-bond between these atoms. This orbital also shows contributions from each rhodium center of 8%, thus accounting for Rh–P–P–Rh multicenter bonding. Orbitals no. 100 and 140 represent the backdonation from a filled d-orbital at Rh into an empty p orbital at one P center (composition: 68% Rh, 22% P). Finally, orbitals no. 194 and 195 describe the same Rh → P backdonation but this time towards the other P atom (main contributions: 57% Rh, 18% P). Additionally, both of these orbitals show some direct Rh–Rh bonding interactions. In summary, this analysis with IBOs allows to describe **4** as a cluster composed from a dicationic $[P{=}P]^{2+}$ fragment coordinated to two Rh^{-1} centers, which strongly donate electron density into this unit.

A related analysis of the electronic structure of **5** with its Rh_4P_4 core of **5** shows that according to the MBOs (0.46, 0.50), all P atoms within the P_4 subunit have substantial bonding interactions but a simple polyphosphide $[P_4]^{4-}$ chain can be excluded (MBOs close to 1 would be expected). Likewise, the MBOs for the Rh–Rh and Rh–P interactions lie within a range of 0.43 to 0.68, which in summary indicate the presence of highly delocalized multi-center bonds between all atoms of the eight-membered cluster (see Tables S2–S4 for a listing of the MBOs).

The number of doubly occupied bonding orbitals within the Rh_4P_4 unit was again determined by examining the intrinsic bond orbitals (IBO). In total, eight orbitals and thus 16

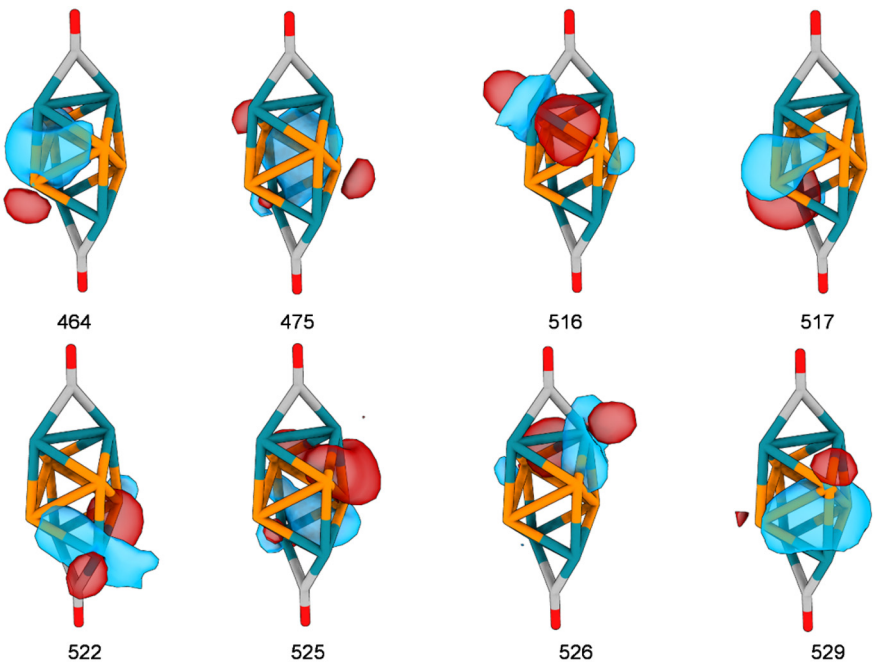

Fig. 3 Orbitals (occupied by two electrons) within the Rh_4P_4 unit accounting for bonding interactions between the cluster atoms (surface isovalue = 0.04, the orbital number is given for each orbital). Color code: C: grey, orange: P, petrol: Rh, red: oxygen.

Table 1 Summary of bond critical point properties in **4** and **5**. In **4**, the average data for the P–Rh bonds was taken, in **5** the average of the data for each kind of bond was taken. ρ: electron density, $\nabla\rho$: Laplacian of the electron density, G: kinetic energy density, V: potential energy density, H: energy density, all values in a.u.

	ρ	$\nabla\rho$	G	V	H
4 (Rh_2P_2)					
P–P	0.126	−0.134	0.0428	−0.119	−0.0763
Rh–Rh	0.0483	0.0709	0.0311	−0.0445	−0.0134
P–Rh	0.080	0.0721	0.0467	−0.0753	−0.0286
5 (Rh_4P_4)					
P–P	0.0538	0.0414	0.0202	−0.0300	−0.0098
Rh–Rh	0.0487	0.1100	0.0368	−0.0461	−0.0093
P–Rh	0.0766	0.0758	0.0446	−0.0702	−0.0256

electrons were found which account for bonding within the Rh_4P_4 unit which are shown in Fig. 3.

For both, **4** and **5**, the electronic structure was further studied using a QTAIM analysis as implemented in the program MultiWFN.[39] In the case of the tetrahedral cluster **4**, six bond critical points within the Rh_2P_2 unit were located, accounting for P–P, Rh–Rh and P–Rh bonding. Commonly analysed properties at those bond critical points are summarized in Table 1. According to established criteria (high electron density, negative Laplacian, magnitude of potential energy density significantly higher than kinetic energy density), the P–P interaction in **4** can be described as covalent bonding, whereas the properties at bond critical points of the Rh–P bonds indicate dative bonding (low electron density, positive Laplacian, magnitude of potential energy density similar to kinetic energy density). Thus, the QTAIM analysis supports the description of **4** as construct between a $[P{=}P]^{2+}$ unit and two $[Rh^{-1}(CO)(Ph_2Ptrop)]$ fragments as derived from the IBO analysis. In case of the eight vertices Rh_4P_4 cluster, 18 bond critical points were found: **4** accounting for P–P bonding, 12 accounting for Rh–P bonding and **2** accounting for Rh–Rh bonding. The descriptors given in Table 1 indicate that all bonding interactions are relatively weak and dative in nature, substantiating the description of the Rh_4P_4 core as a cluster with a highly delocalized electronic structure.

Conclusions

In this paper we show that molecular transition metal phosphido (TMP) clusters can be obtained using sodium phosphaethynolate, Na[OCP], as "P^-" transfer reagent. This approach may be especially interesting for the synthesis of clusters with late transition metal centers and metal to phosphorus ratios which are not easily accessible with protocols borrowed from solid state syntheses. The metal precursor complex is decisive for a successful TMP synthesis: (i) Results to date imply that precursor complexes, which are too strongly oxidizing must be avoided. Otherwise $[OCP]^-$ serves as reductant[15] and not as nucleophile. (ii) The experiments with electronically saturated metal complexes – such as those with the fragments $[Rh(Ptrop_3)]$ or $[Rh(PhPtrop_2)]$ containing a tetradentate or tridentate ligand – suggest that these may lead to stable M(PCO) complexes but a migration of the CO unit requires an open coordination site at the metal. Bonding analyses of the small cluster **4** containing a tetrahedral Rh_2P_2 core and the unprecedented eight-vertices Rh_4P_4 cluster **5** show that the breadth of possible electronic structures observed for binary rhodium phosphor phases is reflected by molecular Rh_nP_m clusters. The cluster $[Rh_2(CO)_2(Ph_2Ptrop)_2(\eta^2\text{-}P_2)]$ **4** obeys the electron counting rules for electron precise clusters and hence **4** is an analogue of tetrahedran, C_4H_4 [that is $b = \frac{1}{2}(18m - 8n) - VEC$ with m = number of transition metal centers, n = number of main group element centers, VEC = valence electron count, b = number of bonds with the $m + n$ cluster necessary to achieve an 18 valence electron count at each transition or 8 valence electron count at each main group element center. For **4** this results in: VEC = (2 × 9 Rh) + (2 × 2 CO) + (2 × 4 Ph_2Ptrop) + (2 × 5 P) = 40; $18m + 8n = 52$; $b = \frac{1}{2}(52–40) = 6$]. On the other hand, cluster **5** with its Rh_4P_4 core held together by a total of eight bonding orbitals can be classified as a hypercloso cluster related to the archetype B_8Cl_8.[40]

Author contributions

J. E. Borger carried out most of the experimental work. Z. Li and P. Coburger carried out the computational studies. The manuscript was written through contributions of all authors. All authors have given approval to the final version of the manuscript.

Conflicts of interest

There are no conflicts to declare.

Data availability

Supplementary information: experimental details, NMR spectra, computational details, single-crystal X-ray structure determinations. See DOI: https://doi.org/10.1039/d5dt02274f.

CCDC 1827127 (**1***), 1827128 (**2**), 1827129 (**4**), 1827130 (**3**), and 1827133 (**5**) contain the supplementary crystallographic data for this paper.[41a–e]

Acknowledgements

This work was supported by the Swiss National Science Foundation (SNF 2-77199-18) and the ETH Zürich (ETH-36 17-2).

References

1 (*a*) B. Owens-Baird, Y. V. Kolen'ko and K. Kovnir, *Chem. – Eur. J.*, 2018, **24**, 7298–7311; (*b*) P. W. Menezes, A. Indra, C. Das, C. Walter, C. Göbel, V. Gutkin, D. Schmeißer and M. Driess, *ACS Catal.*, 2017, **7**, 103–109; (*c*) M. Sun, H. Liu,

J. Qu and J. Li, *Adv. Energy Mater.*, 2016, **6**, 1600087; (*d*) Y. Shi and B. Zhang, *Chem. Soc. Rev.*, 2016, **45**, 1529–1541; (*e*) S. Anantharaj, S. R. Ede, K. Sakthikumar, K. Karthick, S. Mishra and S. Kundu, *ACS Catal.*, 2016, **6**, 8069–8097; (*f*) P. C. K. Vesborg, B. Seger and I. Chorkendorff, *J. Phys. Chem. Lett.*, 2015, **6**, 951–957.

2 (*a*) S. E. Habas, F. G. Baddour, D. A. Ruddy, C. P. Nash, J. Wang, M. Pan, J. E. Hensley and J. A. Schaidle, *Chem. Mater.*, 2015, **27**, 7580–7592; (*b*) M. B. Griffin, F. G. Baddour, S. E. Habas, C. P. Nash, D. A. Ruddy and J. A. Schaidle, *Catal. Sci. Technol.*, 2017, **7**, 2954–2966.

3 (*a*) S. Carenco, D. Portehault, C. Boissière, N. Mézailles and C. Sanchez, *Chem. Rev.*, 2013, **113**, 7981–8065; (*b*) S. Carenco, D. Portehault, C. Boissière, N. Mézailles and C. Sanchez, *Adv. Mater.*, 2014, **26**, 371–390; (*c*) J.-H. Chen and K. H. Whitmire, *Coord. Chem. Rev.*, 2018, **355**, 271–327.

4 (*a*) C. Panda, P. W. Menezes and M. Driess, *Angew. Chem., Int. Ed.*, 2018, **57**, 11130–11139; (*b*) S. Yao, V. Forstner, P. W. Menezes, C. Panda, S. Mebs, E. M. Zolnhofer, M. E. Miehlich, T. Szilvási, N. Ashok Kumar, M. Haumann, K. Meyer, H. Grützmacher and M. Driess, *Chem. Sci.*, 2018, **9**, 8590–8597.

5 (*a*) B. M. Cossairt, N. A. Piro and C. C. Cummins, *Chem. Rev.*, 2010, **110**, 4164–4177; (*b*) M. Caporali, L. Gonsalvi, A. Rossin and M. Peruzzini, *Chem. Rev.*, 2010, **110**, 4178–4235; (*c*) C. M. Hoidn, D. J. Scott and R. Wolf, *Chem. – Eur. J.*, 2021, **27**, 1886–1902.

6 (*a*) S. Rundqvist, *Nature*, 1960, **185**, 31–32; (*b*) F.-E. Faller, E. F. Strotzer and W. Biltz, *Z. Anorg. Allg. Chem.*, 1940, **244**, 317–328.

7 (*a*) C. Xu, Q. Wang, R. Ding, Y. Wang, Y. Zhang and G. Fan, *Appl. Surf. Sci.*, 2019, **489**, 796–801; (*b*) J. Kim, H. Kim and S. H. Ahn, *ACS Sustainable Chem. Eng.*, 2019, **7**, 14041–14050; (*c*) F. Yang, X. Bao, D. Gong, L. Su, G. Cheng, S. Chen and W. Luo, *ChemElectroChem*, 2019, **6**, 1990–1995; (*d*) J.-Q. Chi, X.-J. Zeng, X. Shang, B. Dong, Y.-M. Chai, C.-G. Liu, M. Marin and Y. Yin, *Adv. Funct. Mater.*, 2019, **29**, 1901790; (*e*) H. Xin, L. Sun, Y. Zhao, Y. Lv, Q. Luo, S. Guo, D. Li, C. Mu, B. Huang and F. Ma, *Chem. Eng. J.*, 2023, **466**, 143277; (*f*) B. Guo, J. Zhao, Y. Xu, X. Wen, X. Ren, X. Huang, S. Niu, Y. Dai, R. Gao, P. Xu and S. Li, *ACS Appl. Mater. Interfaces*, 2024, **16**, 8939–8948.

8 Z. Chen, Y. Bu, L. Wang, X. Wang and J.-P. Ao, *Appl. Catal., B*, 2020, **274**, 119117.

9 F. Luo, Y. Yu, X. Long, C. Li, T. Xiong and Z. Yang, *J. Colloid Interface Sci.*, 2024, **656**, 450–456.

10 (*a*) J. R. Hayes, R. H. Bowker, A. F. Gaudette, M. C. Smith, C. E. Moak, C. Y. Nam, T. K. Pratum and M. E. Bussell, *J. Catal.*, 2010, **276**, 249–258; (*b*) Y. Kanda, K. Kawanishi, T. Tsujino, A. M. Al-otaibi and Y. Uemichi, *Catalysts*, 2018, **8**, 160; (*c*) Y. Kanda, R. Saito, T. Ono, K. Kon, T. Toyao, S. Furukawa, Y. Obora and K.-i. Shimizu, *J. Catal.*, 2022, **408**, 294–302.

11 C. Galdeano-Ruano, C. W. Lopes, D. Motta Meira, A. Corma and P. Oña-Burgos, *ACS Appl. Nano Mater.*, 2021, **4**, 10743–10753.

12 C. Lin, J. Zhou, Z. Zheng and J. Chen, *J. Catal.*, 2022, **410**, 164–179.

13 (*a*) G. Becker, W. Schwarz, N. Seidler and M. Westerhausen, *Z. Anorg. Allg. Chem.*, 1992, **612**, 72–82; (*b*) F. F. Puschmann, D. Stein, D. Heift, C. Hendriksen, Z. A. Gal, H.-F. Grützmacher and H. Grützmacher, *Angew. Chem., Int. Ed.*, 2011, **50**, 8420–8423; (*c*) D. Heift, Z. Benkő and H. Grützmacher, *Dalton Trans.*, 2014, **43**, 831–840; (*d*) R. Suter, Z. Benkő, M. Bispinghoff and H. Grützmacher, *Angew. Chem., Int. Ed.*, 2017, **56**, 11226–11231; (*e*) I. Krummenacher and C. C. Cummins, *Polyhedron*, 2012, **32**, 10–13; (*f*) A. R. Jupp and J. M. Goicoechea, *Angew. Chem., Int. Ed.*, 2013, **52**, 10064–10067.

14 (*a*) J. M. Goicoechea and H. Grützmacher, *Angew. Chem., Int. Ed.*, 2018, **57**, 16968–16994; (*b*) L. Weber, *Eur. J. Inorg. Chem.*, 2018, **2018**, 2175–2227.

15 (*a*) D. Heift, Z. Benkő and H. Grützmacher, *Chem. – Eur. J.*, 2014, **20**, 11326–11330; (*b*) A. M. Tondreau, Z. Benkő, J. R. Harmer and H. Grützmacher, *Chem. Sci.*, 2014, **5**, 1545–1554; (*c*) D. Heift, Z. Benkő, H. Grützmacher, A. R. Jupp and J. M. Goicoechea, *Chem. Sci.*, 2015, **6**, 4017–4024; (*d*) T. P. Robinson, M. J. Cowley, D. Scheschkewitz and J. M. Goicoechea, *Angew. Chem., Int. Ed.*, 2015, **54**, 683–686; (*e*) N. Del Rio, A. Baceiredo, N. Saffon-Merceron, D. Hashizume, D. Lutters, T. Müller and T. Kato, *Angew. Chem., Int. Ed.*, 2016, **55**, 4753–4758; (*f*) M. M. Hansmann and G. Bertrand, *J. Am. Chem. Soc.*, 2016, **138**, 15885–15888; (*g*) Z. Li, X. Chen, Y. Li, C.-Y. Su and H. Grützmacher, *Chem. Commun.*, 2016, **52**, 11343–11346; (*h*) L. Liu, D. A. Ruiz, D. Munz and G. Bertrand, *Chem*, 2016, **1**, 147–153; (*i*) S. Yao, Y. Xiong, T. Szilvási, H. Grützmacher and M. Driess, *Angew. Chem., Int. Ed.*, 2016, **55**, 4781–4785; (*j*) T. Krachko, A. W. Ehlers, M. Nieger, M. Lutz and J. C. Slootweg, *Angew. Chem., Int. Ed.*, 2018, **57**, 1683–1687; (*k*) D. W. N. Wilson, A. Hinz and J. M. Goicoechea, *Angew. Chem., Int. Ed.*, 2018, **57**, 2188–2193; (*l*) T. G. Saint-Denis, T. A. Wheeler, Q. Chen, G. Balázs, N. S. Settineri, M. Scheer and T. D. Tilley, *J. Am. Chem. Soc.*, 2024, **146**, 4369–4374.

16 S. Alidori, D. Heift, G. Santiso-Quinones, Z. Benkő, H. Grützmacher, M. Caporali, L. Gonsalvi, A. Rossin and M. Peruzzini, *Chem. – Eur. J.*, 2012, **18**, 14805–14811.

17 L. L. Liu, D. A. Ruiz, F. Dahcheh, G. Bertrand, R. Suter, A. M. Tondreau and H. Grützmacher, *Chem. Sci.*, 2016, **7**, 2335–2341.

18 M. M. D. Roy, M. J. Ferguson, R. McDonald and E. Rivard, *Chem. Commun.*, 2018, **54**, 483–486.

19 (*a*) C. J. Hoerger, F. W. Heinemann, E. Louyriac, L. Maron, H. Grützmacher and K. Meyer, *Organometallics*, 2017, **36**, 4351–4354; (*b*) C. Camp, N. Settineri, J. Lefèvre, A. R. Jupp, J. M. Goicoechea, L. Maron and J. Arnold, *Chem. Sci.*, 2015, **6**, 6379–6384.

20 L. N. Grant, B. Pinter, B. C. Manor, H. Grützmacher and D. J. Mindiola, *Angew. Chem., Int. Ed.*, 2018, **57**, 1049–1052.

21 S. Bestgen, Q. Chen, N. H. Rees and J. M. Goicoechea, *Dalton Trans.*, 2018, **47**, 13016–13024.

22 L. Weber, B. Torwiehe, G. Bassmann, H.-G. Stammler and B. Neumann, *Organometallics*, 1996, **15**, 128–132.
23 W. Lü, C. Wang, Q. Luo, Q.-s. Li, Y. Xie, R. B. King and H. F. Schaefer III, *New J. Chem.*, 2015, **39**, 1390–1403.
24 L. N. Grant, B. Pinter, B. C. Manor, R. Suter, H. Grützmacher and D. J. Mindiola, *Chem. – Eur. J.*, 2017, **23**, 6272–6276.
25 J. Sun, H. Verplancke, J. I. Schweizer, M. Diefenbach, C. Würtele, M. Otte, I. Tkach, C. Herwig, C. Limberg, S. Demeshko, M. C. Holthausen and S. Schneider, *Chem*, 2021, **7**, 1952–1962.
26 J. Du, D. Hunger, J. A. Seed, J. D. Cryer, D. M. King, A. J. Wooles, J. van Slageren and S. T. Liddle, *J. Am. Chem. Soc.*, 2021, **143**, 5343–5348.
27 G. Hierlmeier, A. Hinz, R. Wolf and J. M. Goicoechea, *Angew. Chem., Int. Ed.*, 2018, **57**, 431–436.
28 M. Joost, W. J. Transue and C. C. Cummins, *Chem. Commun.*, 2017, **53**, 10731–10733.
29 (*a*) T. Zweifel, J.-V. Naubron, T. Büttner, T. Ott and H. Grützmacher, *Angew. Chem., Int. Ed.*, 2008, **47**, 3245–3249; (*b*) U. Fischbach, H. Rüegger and H. Grützmacher, *Eur. J. Inorg. Chem.*, 2007, **2007**, 2654–2667; (*c*) F. F. Puschmann, J. Harmer, D. Stein, H. Rüegger, B. de Bruin and H. Grützmacher, *Angew. Chem., Int. Ed.*, 2010, **49**, 385–389; (*d*) H. Schönberg, S. Boulmaâz, M. Wörle, L. Liesum, A. Schweiger and H. Grützmacher, *Angew. Chem., Int. Ed.*, 1998, **37**, 1423–1426.
30 M. J. Frisch, *et al.*, *Gaussian 16, Revision C.01*, 2016.
31 (*a*) F. H. Allen, O. Kennard, D. G. Watson, L. Brammer, A. G. Orpen and R. Taylor, *J. Chem. Soc., Perkin Trans. 2*, 1987, S1–S19; (*b*) P. Pyykkö and M. Atsumi, *Chem. – Eur. J.*, 2009, **15**, 186–197; (*c*) P. Pyykkö and M. Atsumi, *Chem. – Eur. J.*, 2009, **15**, 12770–12779.
32 K. M. Szkop, A. R. Jupp, R. Suter, H. Grützmacher and D. W. Stephan, *Angew. Chem., Int. Ed.*, 2017, **56**, 14174–14177.
33 M. Caporali, L. Gonsalvi, V. Mirabello, A. Ienco, G. Manca, F. Zanobini and M. Peruzzini, *Eur. J. Inorg. Chem.*, 2014, **2014**, 1652–1659.
34 S. Alvarez, *Dalton Trans.*, 2013, **42**, 8617–8636.
35 G. L. Simon and L. F. Dahl, *J. Am. Chem. Soc.*, 1973, **95**, 2175–2183.
36 (*a*) M. Zumbusch, *Z. Anorg. Allg. Chem.*, 1940, **243**, 322–329; (*b*) E. H. El Ghadraoui, R. Guerin and M. Sergent, *Acta Crystallogr., Sect. C: Cryst. Struct. Commun.*, 1983, **39**, 1493–1494.
37 (*a*) F. Neese, F. Wennmohs, U. Becker and C. Riplinger, *J. Chem. Phys.*, 2020, **152**, 224108; (*b*) F. Neese, *Wiley Interdiscip. Rev.:Comput. Mol. Sci.*, 2018, **8**, e1327.
38 (*a*) G. Knizia, *J. Chem. Theory Comput.*, 2013, **9**, 4834–4843; (*b*) W. Sun, X. Xia, C. Lu, X. Kuang and A. Hermann, *Phys. Chem. Chem. Phys.*, 2018, **20**, 23740–23746; (*c*) J. E. M. N. Klein, R. W. A. Havenith and G. Knizia, *Chem. – Eur. J.*, 2018, **24**, 12340–12345; (*d*) M. T. Scharnhölz, P. Coburger, L. Gravogl, D. Klose, J. J. Gamboa-Carballo, G. Le Corre, J. Bösken, C. Schweinzer, D. Thöny, Z. Li, K. Meyer and H. Grützmacher, *Angew. Chem., Int. Ed.*, 2022, **61**, e202205371.
39 T. Lu and F. Chen, *J. Comput. Chem.*, 2012, **33**, 580–592.
40 W. Einholz, M. Hofmann, R. Schäfer, C. Wieloch, W. Keller, M. Ströbele and H.-J. Meyer, *Eur. J. Inorg. Chem.*, 2021, **2021**, 5037–5044.
41 (*a*) CCDC 1827127: Experimental Crystal Structure Determination, 2025, DOI: 10.5517/ccdc.csd.cc1zb8l5; (*b*) CCDC 1827128: Experimental Crystal Structure Determination, 2025, DOI: 10.5517/ccdc.csd.cc1zb8m6; (*c*) CCDC 1827129: Experimental Crystal Structure Determination, 2025, DOI: 10.5517/ccdc.csd.cc1zb8n7; (*d*) CCDC 1827130: Experimental Crystal Structure Determination, 2025, DOI: 10.5517/ccdc.csd.cc1zb8p8; (*e*) CCDC 1827133: Experimental Crystal Structure Determination, 2025, DOI: 10.5517/ccdc.csd.cc1zb8sc.